Polaronic Structure in $La_{1.2}Sr_{1.8}Mn_2O_7$

B.J. Campbell,[1] R. Osborn,[1] S.K. Sinha,[2] D.N. Argyriou,[1] S. Rosenkranz,[1] J.F. Mitchell,[1]
L. Vasiliu-Doloc,[2] O.H. Seeck,[2] U. Ruett,[1] C.D. Ling,[1] Z. Islam,[2] J.W. Lynn[3]
[1]Materials Science Division and
[2]Advanced Photon Source (APS), Argonne National Laboratory, Argonne IL, U.S.A.
[3]NIST Center for Neutron Research (NCNR), National Institute for Standards and Technology (NIST),
Gaithersburg, MD, U.S.A.

Introduction

Colossal magnetoresistive (CMR) phenomena occur in mixed-valence manganite systems, such as $La_{1-x}Ca_xMnO_3$ and $La_{2-2x}Sr_{1+2x}MnO_7$, which exhibit a sharp transition between a high-temperature paramagnetic insulating state and a low-temperature ferromagnetic metallic state. In the insulating state above T_c, the strong coupling of the Mn^{3+} e_g electrons to Jahn-Teller (JT) distortions of the MnO_6 octahedra is essential to the formation of electron-lattice polarons, which are e_g electrons that become trapped within self-induced distortions. These lattice distortions can serve as structural markers that aid in tracking the complex interactions among other (e.g., charge, spin, and orbital) coupled degrees of freedom. High-energy single-crystal x-ray diffuse scattering is a powerful probe of subtle atomic displacements, and it has recently demonstrated that the formation of the metallic state at T_c marks an abrupt loss of polaronic distortions [1-2]. Recent experiments at the SRI-CAT beamline 1-ID and BESSRC beamline station 11-ID-C at the APS now reveal novel polaronic structures in $La_{1.2}Sr_{1.8}Mn_2O_7$ [3-4].

Methods and Materials

Single-crystal x-ray diffuse scattering measurements were performed by using $6 \times 4 \times 1$-mm and $2 \times 2 \times 0.25$-mm single-crystal samples of $La_{1.2}Sr_{1.8}Mn_2O_7$ cleaved from the same region of a boule that was grown by the floating-zone technique. The megapixel diffuse scattering image in Fig. 1 was collected at 125K by using 115-keV x-rays from the BESSRC beamline 11-ID and a Bruker 6500 charge-coupled device (CCD) x-ray camera. The large detector area (270 cm^2), combined with a long sample-to-detector distance of 2.5 m, permit a high-resolution view of the scattering features surrounding the (200) Bragg reflection. Because of the small scattering angle, this image approximately represents a constant k slice of reciprocal space. The Bragg reflection was moved slightly off the Ewald sphere ($k_0 = 0.005$) to prevent saturation during the long exposures required to detect the weaker diffuse scattering features. The highly anisotropic "butterfly-shaped" scattering pattern [1-2] at the center of the figure is associated with strain-fields induced by local

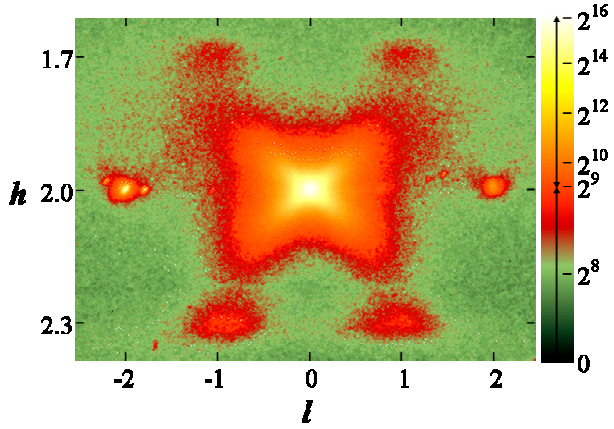

FIG 1. X-ray single-crystal diffuse x-ray scattering data (115 keV) in the $k_0 = 0$ *plane simultaneously reveal polaron correlations, anisotropic Huang scattering, and thermal diffuse scattering near the (200) Bragg reflection. The intensity scale of this CCD image is logarithmic.*

JT distortions and is commonly referred to as Huang scattering [5]. Temperature-dependent mesh scans through several of these butterfly scattering features were collected by using 36-keV x-rays and a Ge solid-state detector at SRI-CAT beamline 1-ID. The four diffuse satellite maxima [1] near (2 ±0.3, 0, ±1) indicate nanoscale polaronic spatial organization. The intensities of more than 100 of these diffuse satellites were also measured at the SRI 1-ID beamline. Because the peak widths did not vary significantly from satellite to satellite, a simple *h*-scan through the center of each peak was sufficient to determine the integrated intensities, which were then subjected to crystallographic analysis via the JANA software package [6].

Results and Discussion

The inverted connection between real and reciprocal space requires that the structure near the core of a polaronic distortion be encoded into scattering features that are widely dispersed in reciprocal space. Information about a polaron's long-range structural influence, on the other hand, is concentrated into features immediately

surrounding the Bragg peaks, making it much easier to measure. The butterfly scattering in Fig. 1 is essentially the Fourier transform of the long-range crystal strain field that extends outward from a polaronic distortion. By force-coupling the long-range elastic strain field to the atomic displacements that make up the local distortion, a 3-D model of the local structure is obtained, which would ordinarily be very difficult to probe. Conceptually, we (a) treat the crystal as a continuous elastic medium, (b) embed an MnO_6 octahedron into the medium, (c) apply balanced forces to the apical oxygens, (d) allow the medium to respond to this local distortion by forming a long-range strain field, and then (e) calculate the diffuse scattering due to this strain field.

Calculated (at room temperature) and experimental butterfly scattering features appear in Fig. 2. The adjustable parameters in the calculated fit to the experimental data are the three independent Mn-O bonds of a single JT-distorted MnO_6 octahedron. The distortion parameters are made quantitative by using the thermal diffuse scattering contribution to the butterfly pattern as an internal reference. Far above T_C, the elongated JT-distorted MnO_6 octahedra are found to be preferentially oriented perpendicular to the double-perovskite sheets (along *c*) of the material. As the sample is cooled toward T_C, however, the preferred elongation direction is observed to rotate into the (*a*-*b*) plane, even though the internal structure of the distortion does not change dramatically.

As the transition is approached from above, the broad satellite maxima from Fig. 1 grow in intensity, as evidence of developing spatial correlations. Although the diffuse satellites are quite broad (Γ of ~3 nm) and several orders of magnitude weaker in intensity than the parent Bragg peaks, they are sufficiently well-defined to reliably determine their integrated intensities. They correspond to a 1-D modulation that breaks the *I4/mmm* symmetry of the parent structure, and they exhibit systematic absences governed by the (3+1)-dimensional centering condition: $h+k+l+m = 2n$. It is important to note that only first-order satellite maxima (i.e., $m = \pm 1$) are observed. Thus, they only appear adjacent to the $h+k+l = 2n+1$ positions. This set of systematic absences leads to the selection of $Xmmm(\alpha 00)000$ as the (3+1)-dimensional superspace-group symmetry, where *X* refers to the extended body-centering condition — $(x,y,z,t) \rightarrow (x+1/2,\ y+1/2,\ z+1/2,\ t+1/2)$ — and implies that the modulated displacements in adjacent perovskite bilayers are 180° out of phase.

The structure in Fig. 3 illustrates the results of an $|F|^2$ refinement of the modulation amplitudes against the measured satellite intensities, which yielded a weighted agreement factor of 16.3%. Only the u^s_x and u^c_z terms are permitted by symmetry [7], and both were essential for obtaining a good fit to the measured intensities. The elongation of the Mn-O(3a) bonds at position A in the figure is interpreted as a cooperative JT distortion caused by the occupation of Mn e_g orbitals with $d(3x^2-r^2)$ character. These Mn-O(3a) bond distortions are much more pronounced than any of the others. Other cooperative features include the stacking of JT-distorted octahedra within a bilayer, the *c*-axis compression of octahedra that experience *a*-axis elongation, octahedral rotations about the *b* axis, and the 180° phase difference between the modulations in adjacent bilayers, all of which appear to work together to minimize the lattice strain induced by the dominant Mn-O(3a) distortions. The incommensurate $q \approx (0.3,0,\pm 1)$ modulation that emerges

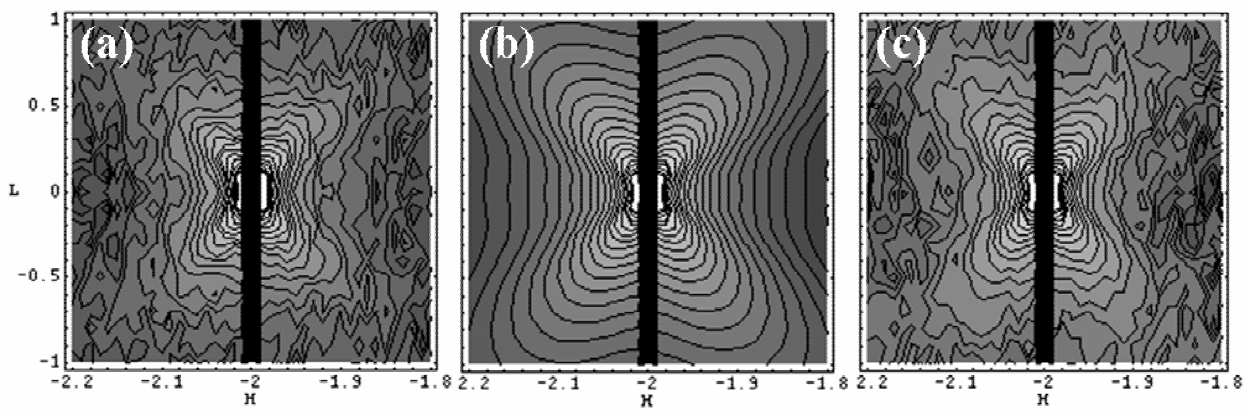

FIG. 2. Calculated and experimental x-ray diffuse scattering data from the (h 0 l) sections surrounding the (2 0 0) Bragg reflection. Panels (a) and (b) contain the experimental and calculated patterns, respectively. Panel (c) is the calculated pattern plus artificial *noise for a more realistic comparison.*

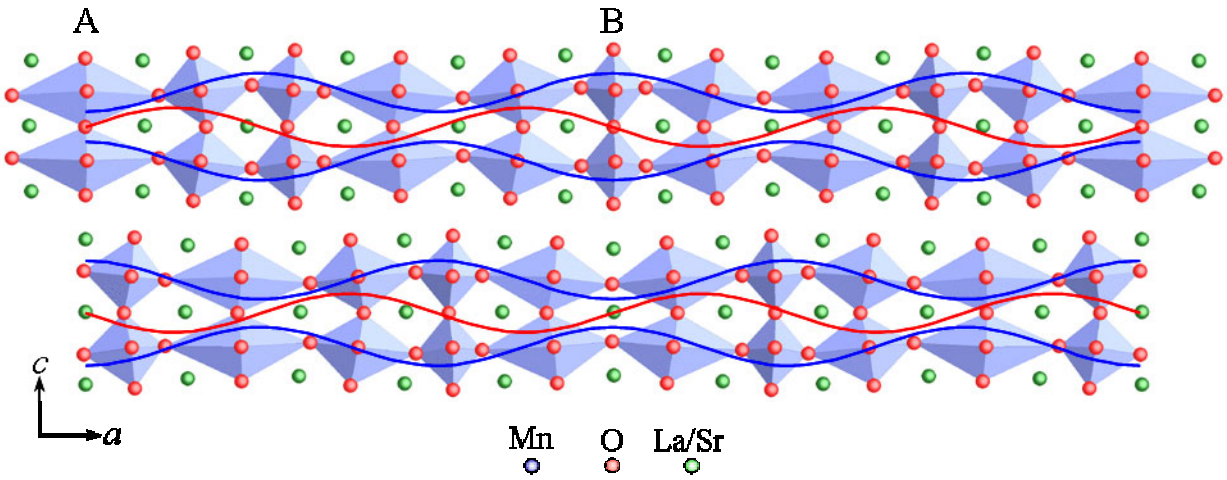

FIG. 3. Crystallographic representation of the incommensurate modulation associated with the diffuse (0.3,0,±1) satellites. Atomic displacements are exaggerated for visual clarity. The directions of the atomic displacements within each perovskite sheet and bilayer follow the blue (z-component) and red (x-component) curves, where peaks indicate +x or +z displacements and troughs indicate –x or –z displacements.

is a longitudinal octahedral stretch mode, and it is structurally consistent with a nanoscale JT-coupled charge-density-wave fluctuation. This observation is corroborated by recent angle-resolved photoemission spectroscopy measurements and local spin density approximation (LSDA) calculations [8] that reveal pronounced Fermi-surface nesting features in the metallic phase below T_c, with a nesting vector $2q_F$ of ≈(0.3,0,±1). A longitudinal modulation of this nature has not been observed in the 3-D CMR manganites [9-11] and may be unique to lower-dimensional systems.

The diffuse scattering data from the SRI-CAT and BESSRC insertion device beamlines provide structural evidence of orientational elongation-axis order associated with orbital polarization and JT-coupled charge density waves in $La_{1.2}Sr_{1.8}Mn_2O_7$. These results demonstrate the utility of high-energy x-ray diffuse scattering as a quantitative probe of polaronic structure.

Acknowledgments

This work was supported by the U.S. Department of Energy (DOE), Office of Science, under Contract W-31-109-ENG-38 and by the State of Illinois under the Higher Education Cooperation Act (HECA). We also acknowledge V. Petricek for assistance with the JANA software, J. Phillips for assistance with the CCD camera at beamline station 11-ID-C, and helpful discussions with R. Klemm, M. Norman, and D. Dessau. Use of the APS was supported by the DOE Office of Science, Office of Basic Energy Sciences, under Contract No.W-31-109-ENG-38. The source of this paper is References 3 and 4 below.

References

[1] L. Vasilu-Doloc, S. Rosenkranz, R. Osborn, S.K. Sinha, J.W. Lynn, J. Mesot, O.H. Seeck, G. Preosti, A.J. Fedro, J.F. Mitchell, Phys. Rev. Lett. 83, 4393 (1999).

[2] Shimomura, N. Wakabayashi, H. Kuwahara, Y. Tokura, Phys. Rev. Lett. 83, 4389 (1999).

[3] B.J. Campbell, R. Osborn, D.N. Argyriou, L. Vasiliu-Doloc, J.F. Mitchell, Z. Islam, C.D. Ling, S.K. Sinha, and J.W. Lynn, Phys. Rev. B 65, 014427 (2002).

[4] B.J. Campbell, S.K. Sinha, R. Osborn, S. Rosenkranz, J.F. Mitchell, D.N. Argyriou, L. Vasiliu-Doloc, O.H. Seeck, and J.W. Lynn, Phys. Rev. B 67, 020409(R) (2003).

[5] K. Huang, Proc. R. Soc. London, Ser. A 190, 102 (1947); P.H. Dederichs, J. Phys. F 3, 471 (1973).

[6] V. Petricek and M. Dusek, *JANA 2000* (Institute of Physics, Praha, Czech Republic, 2000).

[7] V. Petricek and P. Coppens, Acta Crystallogr. A 44, 1051 (1988).

[8] Y.-D. Chuang, A.D. Gromko, D.S. Dessau, T. Kimura, and Y. Tokura, Science 292, 1509 (2001).

[9] S.J.L. Billinge, R.G. DiFrancesco, G.H. Kwei, J.J. Neumeier, and J.D. Thompson, Phys. Rev. Lett. 77, 715 (1996).

[10] C.P. Adams, J.W. Lynn, Y.M. Mukovskii, A.A. Arsenov, and D.A. Shulyatev, Phys. Rev. Lett. 88, 3954 (2000).

[11] P.-C. Dai, J.A. Fernandez-Baca, N. Wakabayashi, E.W. Plummer, Y. Tomioka, and Y. Tokura, Phys. Rev. Lett. 85, 2553 (2000).